Comparison of Cloud Droplet Number Concentrations derived from Remote Sensing Observations and Köhler Theory based Activation Parameterizations

by

Fabian Schmidt-Ott

Additional Master Thesis
January 2019

TU Delft

ABSTRACT

In the present research, the activation parameterization method introduced by Nenes and Seinfeld (2003) was compared and evaluated to a remote sensing-based method by Rusli, Donovan & Russchenberg (2017) for determining the cloud drop number concentration. Both methods have fundamentally different approaches for indirectly determining the cloud droplet number concentration. The parameterization method is based on the Köhler Theory, in which the activation process of particles contained in a rising parcel is modelled for predicting the number concentrations of cloud droplets. The remote sensing method, on the other hand, applies theories about particle-light interactions. Since the remote sensing method determines the cloud droplet concentrations in a more direct manner than the parameterization method, it is regarded here as the reference. An agreement was found between the two models, with a relative error of cloud droplet number concentrations between 41.1% and 78.0%, which lead to errors of the cloud's scattering intensity in the range of 13% and 26%. Despite some discrepancies between the obtained droplet concentrations, the parameterization model shows similar trends to the remote sensing observations. It was found that the updraft velocity that is needed as input variable for the parameterization model has the largest influence on the model's prediction of droplets concentrations, and that it is likely to be an important cause for the seen discrepancies. Furthermore, the present research shows how assumptions were made on the size distribution input variable used in the parameterization model, which were not available from observations.

1. INTRODUCTION

The atmospheric aerosol has a net cooling effect on the global radiation budget, and therefore partly counteracts the global increase of temperature that is caused by increased greenhouse gas concentrations. Aerosol particles can act as cloud condensation nuclei (CCN), which means that they induce the formation of cloud droplets. The concentration of the atmospheric aerosol therefore strongly influences the cloud droplet number concentration (CDNC) and therewith affect the radiative properties of clouds (also referred to as the aerosol indirect effect). An increase in the aerosol concentration should, theoretically, increase the number of cloud droplets. If the number of cloud droplets increases while the cloud contains a constant amount of liquid water, the radius of the droplets decreases, increasing the overall albedo and optical thickness of the cloud (Twomney, 1977). The aerosol-cloud interaction is complex, and it contributes to the largest uncertainty on earth's climate predictions (IPCC, 2014).

Both natural and anthropogonic particle sources contribute to the composition of the atmospheric aerosol. Examples of natural sources are the ocean (sea salt), volcanoes, land biota and soils. Anthropogenic particles are emitted mainly by the industry, fissile fuel combustion (soot) and agriculture (Griffin, 2013). These particles may move upwards, and during the vertical transport of these particles, adiabatic expansion occurs, because the pressure is lower at higher altitudes. Due to the Joule-Thomson-effect, this causes cooling and therewith supersaturation (Joule & Thomson, 1852; Cimatti, 1991). Under sufficiently high supersaturation, these particles can be activated to act CCNs and therewith initiate the formation of cloud droplets (Köhler, 1936). The magnitude of supersaturation is higher as vertical velocity increases (Nenes et al., 2001). The higher the supersaturation, the more smaller and low-hygroscopicity particles can be activated, as will be explained in detail in the following. Since the process of particle activation is relatively well understood, described by Köhler 's Theory, the composition of the aerosol at ground level can therefore be linked to the droplet concentrations in liquid water clouds.

1.1 Köhler Theory

The activation of aerosol particles depends on the size, chemical composition, number concentration and the ambient supersaturation of water vapor (Köhler, 1936). Whereas homogeneous nucleation considers the spontaneous nucleation of water vapor into droplets, heterogeneously activated droplets form through condensation on a CCN (Yau & Rogers, 1989). Heterogeneous particle activation is accurately represented in Köhler's theory, which describes the condensational growth on a dry particle at given supersaturations, and determines whether this one is activated into a cloud droplet. Köhler's relationship between supersaturation and particle size is composed of both the Kelvin effect and Raoult's law.

The equilibrium saturation is given as:

$$S_{eq} = \frac{A}{D_p} - \kappa \frac{d_p^3}{{D_p}^3} \ , \qquad \text{Eq. 1}$$

where κ is the hygroscopicity parameter, D_p and d_p is the wet and dry diameter of the droplet, respectively, and A is the Kelvin coefficient,

$$A \equiv \frac{2M_w\sigma}{RT\rho_w}, \qquad \text{Eq. 2}$$

where σ is the surface tension, T is the temperature, M_W is the molecular weight of water, r_W the density of liquid water and R is the ideal gas constant for water vapor (Zieger et al., 2013).

The Kelvin term in the equation, $\frac{A}{r}$ takes into account the curvature the droplet (Thomson, 1872). The curvature of droplets has an effect on the saturated vapor pressure of the droplet. For a droplet with a high curvature (small droplets), the vapor pressure is higher than for a droplet that has a low curvature (large droplets). This is due to the fact that different curvatures of droplet surfaces lead to different surface tensions (a small curvature means that each molecule at the surface has less direct neighbors, and is therefore more likely to evaporate). For different droplet sizes this results in different condensation/vaporization rates and therefore in different vapor pressures. If the partial pressure of water vapor in the environment is larger than the vapor pressure of the droplet, then there is a net flux of water vapor towards the droplet and the droplet will experience net condensational growth. If the partial pressure of water vapor in the environment is smaller than the vapor pressure of the droplet, then the droplet will evaporate and shrink.

Raoult's term in the equation, $\frac{\kappa r_d^3}{r^3}$ on the other hand describes the effect of chemical composition on vapor pressure. This law states that the vapor pressure over an aqueous solution (assuming that it has a flat surface) is always lower than the vapor pressure over a surface of pure water. Water that contains dissolved substance creates more intermolecular forces and therefore keep water from evaporating. Therefore, different droplet compositions have a different vapor pressures, and they grow with different rates (Zieger et al., 2013).

The resultant Köhler curve describes the equilibrium particle size at different supersaturations. The equilibrium size is the size that neither grows nor shrinks at a particular supersaturation. Fig. 1 shows an example for the growth of an NaCl particle with a dry diameter of 50 nm. The curve shows that the solution effect dictated by Raoul's law dominates for small particle diameters (since, at smalls droplet sizes, the concentration of dissolved substance is much larger than it is at large sizes), and that Kelvin's curvature effect dominates for large diameters. At saturation ratios below 1, the growth is small. If the relative humidity is increased to supersaturation levels, the droplet will grow with rising supersaturation until it reaches its critical size (r_{crit}) with corresponding critical supersaturation (S_{crit}) at the peak of the Köhler

curve. Above this size, the droplet is called activated. If, from this point, the relative humidity drops, the particle will reside in equilibrium at the corresponding saturation ratio on the left side of the peak. However, if the relative humidity slightly exceeds S_{crit}, it enables the droplet to grow even larger than r_{crit} and consequently the droplet will undergo an inhibited growth, assuming that the single NaCl particle consumes negligible amounts of water vapor and therefore doesn't influence the level of supersaturation. (Yau & Rogers, 1989; Zieger et al., 2013)

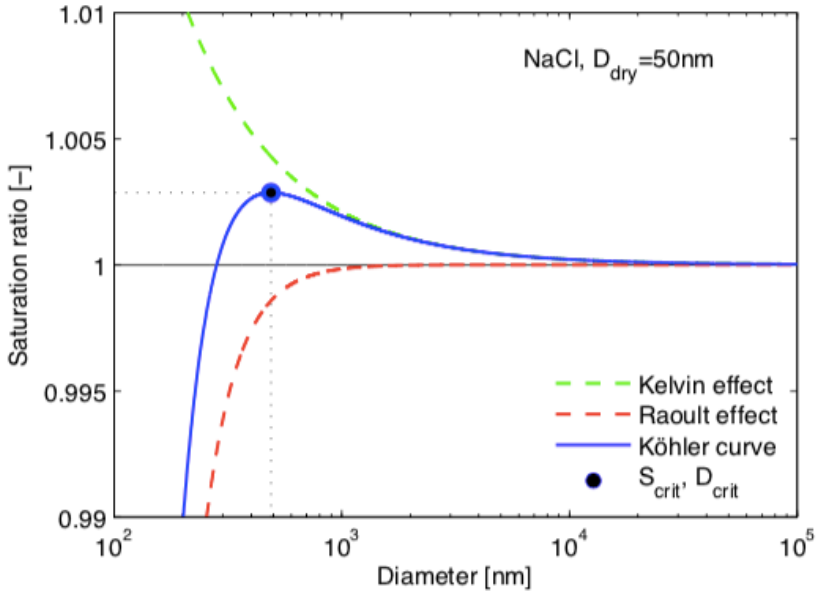

Figure 1. Köhler relationship between the supersaturation and the droplet diameter, visualizing the composition of the curve into the Kelvin and Raoult effect (Zieger et al., 2013).

In reality, however, the process is more complicated, because there are numerous particles that act as a CCN, which means that the ambient supersaturation is influenced by the growth of the particles. Each of these particles has a different composition and size (see Fig. 2), and the CCN particles will compete to draw water vapor to themselves at a different rate, depending on their size and composition (large and hygroscopic particles growing the fastest). Due to the collective consumption of water vapor, the growth is in reality not uninhibited and will therefore stop as soon as the supersaturation has equilibrated to a maximum value (S_{max}). This causes droplets to reside inside the cloud instead of growing to raindrop sizes, and consequently a cloud droplet number concentration establishes inside the cloud, that has several interesting effects on climate (Ghan et al., 2011).

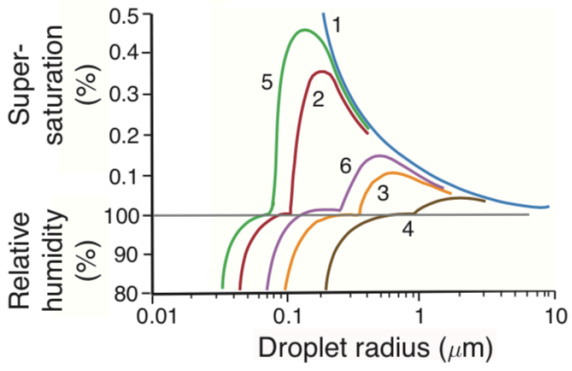

Figure 2. Köhler curves for droplets of different composition and size (represented in mass). 1: pure water, 2: 10^{-19} kg NaCl, 3: 10^{-18} kg NaCl, 4: 10^{-17} kg NaCl, 5: 10^{-19} kg $(NH_4)_2SO_4$, 6: 10^{-18} kg $(NH_4)_2SO_4$ (Wallace & Hobbs, 2006)

1.2 Measurement of cloud droplet number concentration

Cloud droplet number concentrations can be measured in situ with airplanes, which has been done in several measurement campaigns (Snider et al, 2003). However, in order to study the clouds for climate models, in-situ measurements are not suitable, because they are expensive and they give a low spatial coverage of cloud droplet number concentrations.

Another method that is commonly used are numerical parcel models (Peng et al., 2005; Meskhidze et al., 2005; Fountoukis et al, 2007). The essence of parcel models is to determine the cloud droplet number concentration by indirectly deriving it from ground-based measurements of particle number concentrations. Calculations of cloud droplet number concentrations are based the assumption that air parcels rise with a constant velocity towards the cloud base. The parcel experiences adiabatic expansion and therefore at some point the relative humidity within the parcel reaches the critical supersaturation that is needed for particles to become activated. As shown in the Köhler Theory, the droplet growth depends on the size of the particles. Since the size distribution input is taken from ground level measurements, an important assumption is that the size distribution doesn't change on the way up.

Nenes activation parameterizations

The process of new droplet formation and the subsequent growth of the newly formed droplets occurs on sub-grid scales. Calculation of cloud droplet number concentration in atmospheric parcel models is therefore computationally expensive if done explicitly numerically.

Nenes & Seinfeld (2003) developed parameterizations of cloud droplet formation that provide shortcuts and make the computations less expensive. The following theoretical explanations are based on Nenes & Seinfeld (2003), Morales Betancourt et al. (2014) and Ghan et al. (2011).

Computations with these parameterizations consider a Lagrangian-parcel-model approach, in which an air parcel that contains particles ascends with an updraft velocity (w). During the ascent, the parcel adiabatically expands, causing the temperature to gradually decrease. Assuming that no exchange with its environment occurs (adiabatic process), the parcel's vapor pressure exceeds the saturation vapor pressure at the given temperatures (Clausius Clapeyron), causing a supersaturation to establish. The rate of change in supersaturation in the parcel is given as:

$$\frac{dS}{dt} = \alpha w - \gamma \left(\frac{dq_l}{dt}\right), \qquad \text{Eq. 3}$$

where α is the adiabatic expansion parameter, so that the first term stands for cooling by adiabatic expansion by moving upwards with the velocity w. Both α and γ (see Appendix) are slowly varying, size-independent functions that vary with temperature, and they can be regarded

as almost constant during droplet activation. (dq_l/dt) is the rate of change of the liquid water content in the parcel (q_l), which is equal to the depletion rate of water vapor through condensation, which reduces the supersaturation rate. At small t, the adiabatic cooling term is dominant with respect to the depletion of water vapor by condensation, and therefore dS/dt is in the beginning positive. As time progresses, the second (condensational) term gradually increases, as a larger amount of total surface area for condensation becomes available as the droplets continue to grow. Eventually, the condensational term becomes dominant. This implies that there exists a maximum supersaturation (S_{max}), which can be found by setting dS/dt = 0. The maximum supersaturation can be expressed as:

$$S_{max} I(0, S_{max}) = \beta \qquad \text{Eq. 4}$$

where I(a,b) is the condensation integral over the lower (a) and higher (b) saturation limits respectively (see Appendix), and

$$\beta = \frac{2\rho_a \alpha w}{\pi \rho_w \gamma G} \ , \qquad \text{Eq. 5}$$

with mass-transfer coefficient G (see Appendix), ρ_a and ρ_w the densities of air and water.

Equation 4 cannot be integrated analytically in order to obtain S_{max}. However, from Eq. 4 and 5 it can be seen that for a higher updraft velocity (w), the maximum supersaturation (S_{max}) must increase (Morales Betancourt et al., 2014).

The maximum supersaturation in the parcel is of importance for the computation of new cloud droplet formation. From the ground-measured particle size distribution and the hygroscopicity that are provided as input for the model, the availability of CCNs is computed as a function of S_{max} by using Köhler's theory. Only the particles for which $S_{crit} < S_{max}$ eventually become activated into cloud droplets. In Nene's model, the number of activated particles is computed by dividing the aerosol into size sections that are defined by the size distribution, $n^d(D_p)$:

$$n^d(D_p) = \frac{dN}{dD_p} = \frac{N_m}{D_{p,m} - D_{p,m-1}} \qquad \text{Eq. 6}$$

where N is the number of particles, D_p is the particle diameter, and $D_{p,m}$ and $D_{p,m-1}$ are the upper and lower limits of each section (m) respectively.

Using Köhler's theory, the corresponding critical supersaturation distribution, n^s (s), defined by

$$n^s(s) = \frac{dN}{ds} = \frac{N_i}{s_{c,i} - s_{c,i-1}}, \ s_{c,i-1} \leq s \leq s_{c,i} \qquad \text{Eq. 7}$$

where $s_{c,i-1}$ and $s_{c,i}$ are the critical supersaturations corresponding to the boundaries of section i. This leads to the CCN spectrum, which is the particle concentration with critical supersaturation

smaller than s. From the maximum supersaturation the rising parcel obtains, S_{max}, the number of CCN that will be activated (N_d) is given by

$$N_d = F^s(s_{max}) \quad \text{Eq. 8}$$

where F^s is the CCN spectrum. The maximum parcel supersaturation is derived considering that the supersaturation increases from the cooling of the parcel (Joule-Thomson effect), but condensation onto the activated droplets depletes water vapor in the cloud, which pulls the supersaturation downwards (Eq. 3).

The simulations done in the present research were done with the help of Dimitra Mamali, who translated the original Fortran code to Matlab for her current PhD research. In the following, the cloud droplet concentration determined by Nenes parameterization method will be referred to as "Nenes CDNC".

Remote sensing observations

A more direct method of measuring the cloud droplet number concentration is the use of ground-based remote sensing devices. An advantage of remote sensing techniques for determining the cloud droplet number concentration is that they determine the cloud properties with a high spaciotemporal resolution. A method has been developed by Rusli, Donovan & Russchenberg (2017) combines microwave radiometers, radar and lidar measurements to determine the cloud droplet number concentration. Besides having a high tempo-spatial resolution, the combination of different remote sensing techniques allows to obtain cloud droplet number concentrations of both drizzling and non-drizzling clouds. Due to the different frequency windows that the devices operate with, they are able to retrieve more detailed information about the cloud and are therefore able to distinguish the drizzle within the cloud (assumed to be droplets above 12 um) from the cloud droplets. In the following, the cloud droplet number concentration determined by the remote sensing observations will be referred to as "remote sensing CDNC".

1.3 Goal of the present research

The purpose of the current research is to find and evaluate discrepancies between the results of cloud droplet number concentrations obtained from the remote sensing measurements and those predicted by the parameterization model by Nenes, using observations from Cabauw. Since the remote sensing method is a more direct approach for measuring the cloud droplet number concentration than the parameterization method, it will be regarded in the following as the reference. The discrepancies between the obtained cloud droplet number concentrations will be addressed by discussing some assumptions that the Nenes model is based on.

An ideal comparison is not possible, because measurements of particle number concentrations that are needed for Nenes' model are not available during the timeframes in which CDNC data are available from the remote sensing model. For this purpose, a particle size distribution was assumed, based on existing measurements on previous days. A further point that will be addressed is therefore, how an appropriate assumption for the size distribution for that time frame can be made.

The research questions are thus the following: What are sensible assumptions for the particle number concentrations during a timeframe in which the CCN concentration has been derived by remote sensing? How do the predictions from the Nenes model based on Cabauw data compare with the remote sensing result for the CCN concentration? If there are deviations in the comparison above, how can these qualitatively be explained?

2. METHODS

2.1 Sampling site

The measurements were done at the Cabauw Experimental Site for Atmospheric Research (CESAR) in the month of October 2014 during the ACCEPT campaign. The measuring station of Cabauw is located in The Netherlands, in a rural area surrounded by big cities such as Rotterdam (20 km), Utrecht (25 km), Amsterdam (45 km) and The Hague (50 km). It is situated 500 m north of a provincial 1-lane highway, and it receives maritime air masses from the North Sea that is 50 km northwest. Fig. 3 shows a satellite view of its location.

Figure 3. Map of The Netherlands indicating the location of the CESAR measuring station.

2.2 Parameterization model inputs

Inputs needed for the parameterization model are: aerosol size distribution, updraft velocity (w), particle hygroscopicity (κ), temperature, pressure and relative humidity. All inputs, except for the updraft velocities are measured at ground level. From all data 10-minute averages were taken.

Aerosol size distribution

A Scanning Mobility Particle Sizer (SMPS, TSI Model 3034) was installed to measure the size distribution of atmospheric particles. The device measures particle number concentrations over 70 bins that range from 9.37 to 516nm, with a 5 minutes time resolution.

One of the inputs for Nenes' parameterization model is the aerosol size distribution. Since measurements of size distributions are not available for the period in which the remote sensing CCN data are known, 25 and 26 October 2014, a size distribution for these dates was approximated. The approximated size distribution is based on statistical data of size distributions that were measured on the previous days, 18, 19 and 20 October. For each of these 1-hour averaged measurements, a lognormal function in the form of $dN/d\log d_p(d_p)$ was fitted through the data, from which the size distribution parameters were determined (see example in Fig. 4).

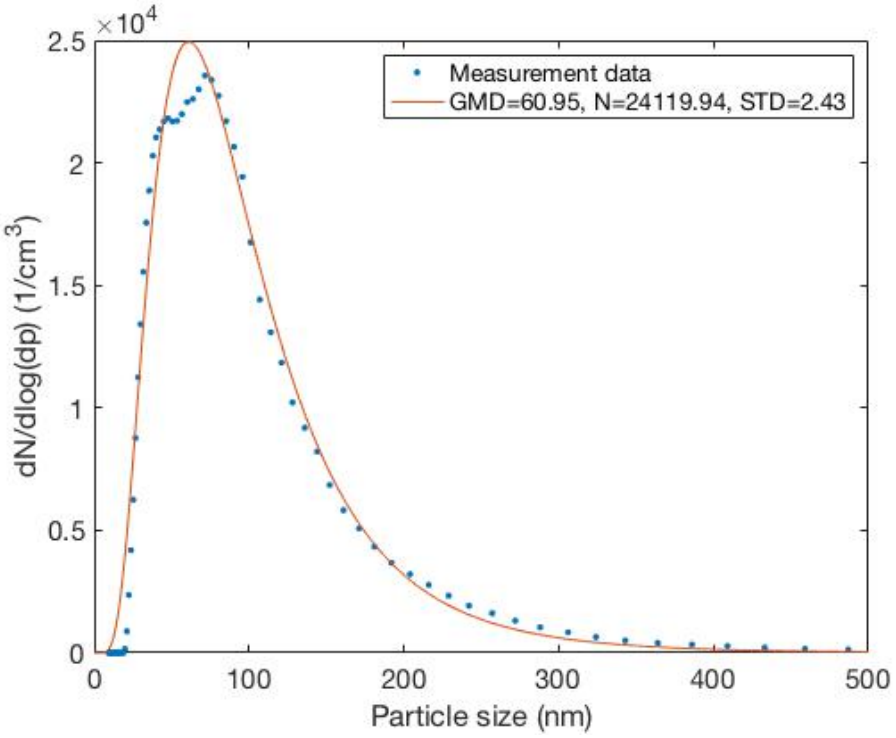

Figure 4. Example of a size distribution with its lognormal fit and the determined parameters. The distribution was measured on 19 October 2014 at 00:00. Geometric mean diameter (GMD), total number concentration (N) and standard deviation (STD) of the curve are calculated from the lognormal fit. See Appendix for examples of two less perfect fits.

Lognormal functions are chosen to fit the size distributions, because they are often encountered in atmospheric aerosols. According to Friedlander (1977), aerosols tend to approach a self-preserving lognormal size distribution.

The period between the dates on which size distributions are available and the dates that are considered for the presented comparison is 5 days. The main assumption made is that the size-composition of the aerosol does not change considerably during this the 5-day period, and that therefore the size distribution defining parameters stay within a limit.

The parameters of a lognormal function in the form of dN/dlog dp (dp) are the geometric mean diameter (GMD), the standard deviation (STD) and the total number concentration (N), as shown in Eq. 9.

$$dN/dlog(dp) = \frac{N}{\sqrt{2\pi}\ln\sigma}\exp\left(-\frac{(\ln d_p - \ln GMD)^2}{2(\ln STD)^2}\right) \quad \text{Eq. 9}$$

From the available size distributions, the average of these parameters was computed. Based on their temporal variations, upper and lower boundaries were derived. It is assumed that the true parameters of the size distributions on 25 and 26 October (on which size distribution data are unavailable) lie within these boundaries.

Fig. 5a to c show the time evolution of these lognormal parameters over the hourly measurements of 18, 19 and 20 October.

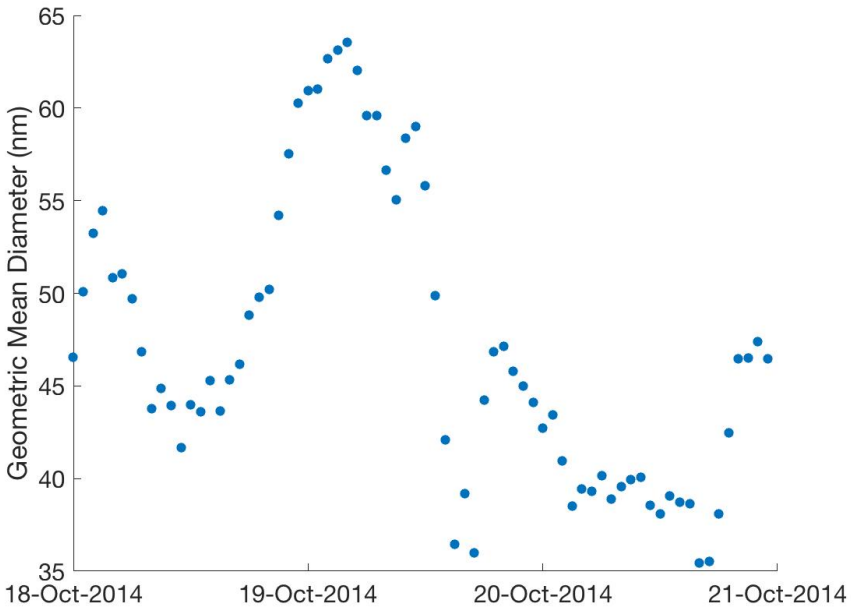

Figure 5a. Evolution of the geometric mean diameter.
μ_{GMD} = 47.1 nm, σ_{GMD} =7.9 nm

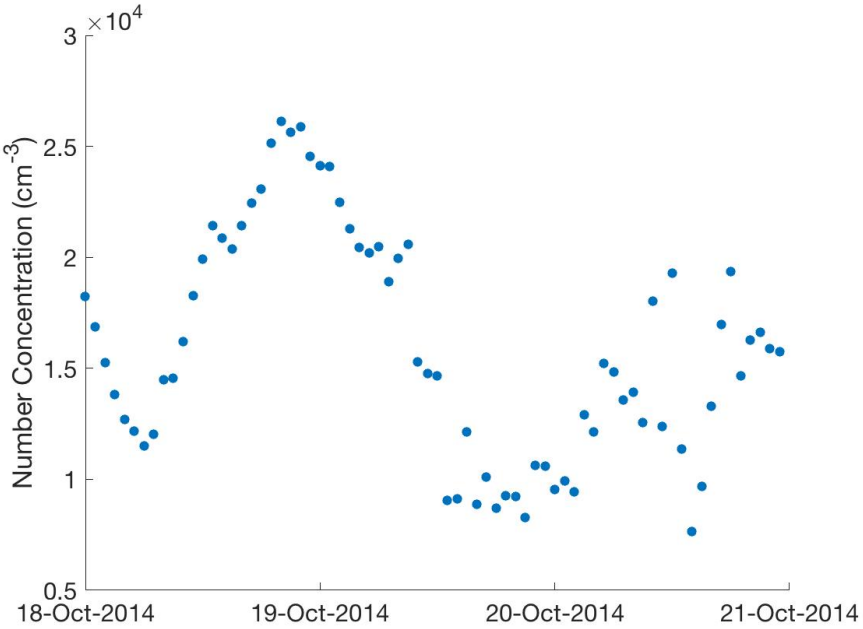

Figure 5b. Evolution of the total number concentration for particle sizes between 9.37 and 516nm.
$\mu_N = 1.6 \times 10^4$ cm^{-3} , $\sigma_N = 5.1 \times 10^3$ cm^{-3}

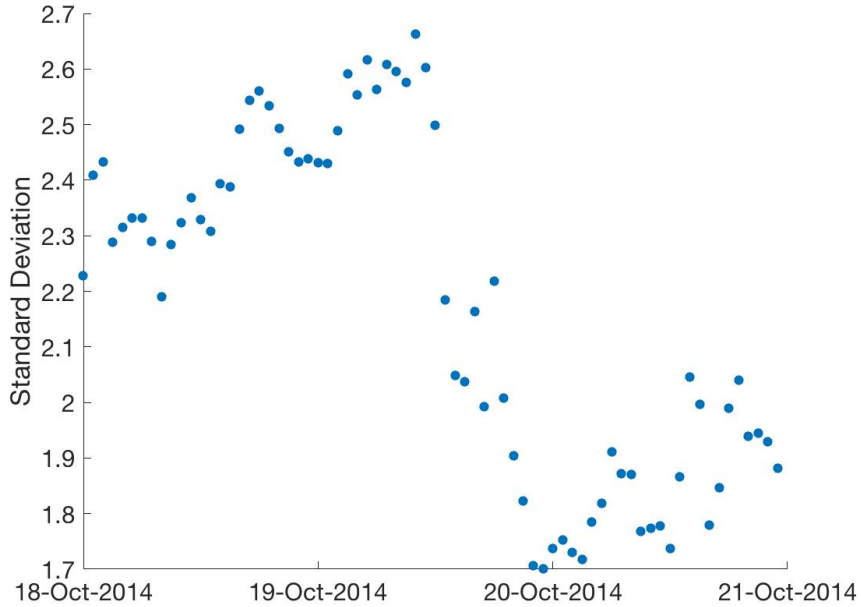

Figure 5c. Evolution of the relative standard deviation.
$\mu_{STD} = 2.2$, $\sigma_{STD} = 0.3$

For each of the parameters, an upper boundary was determined by adding the standard deviation of the series of measurements to the mean of the parameter, and the lower boundary was determined by subtracting the standard deviation from the mean of the parameter, as shown below:

$$upper_{(GMD, N, STD)} = \mu_{(GMD, N, STD)} + \sigma_{(GMD, N, STD)} \quad \text{Eq. 10a}$$

$$lower_{(GMD, N, STD)} = \mu_{(GMD, N, STD)} - \sigma_{(GMD, N, STD)} \quad \text{Eq. 10b}$$

Köhler's theory indicates that at a constant supersaturation and hygroscopicity, large particles are more prone to be activated than small particles. Since size distributions with a large σ_{STD} are wider and therefore also contain more large particles than size distributions with small σ_{STD}, it is expected that a large σ_{STD} contributes to more formation of cloud droplets. With the same reasoning, size distributions with a large GMD are associated with a large number of cloud droplets. Furthermore, a large N increases the number of possible CCNs and therefore also contributes to a higher cloud droplet number concentration. For this reason, the size distributions that cause the maximum amount of cloud droplets are composed of upper(GMD), upper(N) and upper(σ_{sd}). According to the same reasoning, the minimum amount of cloud formation follows from the size distribution with low boundary lower(GMD), lower(N) and lower(σ_{sd}). Fig. 6 shows the boundary distributions that were found by applying these combinations of parameters to form two lognormal curves. The blue and the red curve induce a maximum and a minimum of CDNC respectively when applied to the model of Nenes.

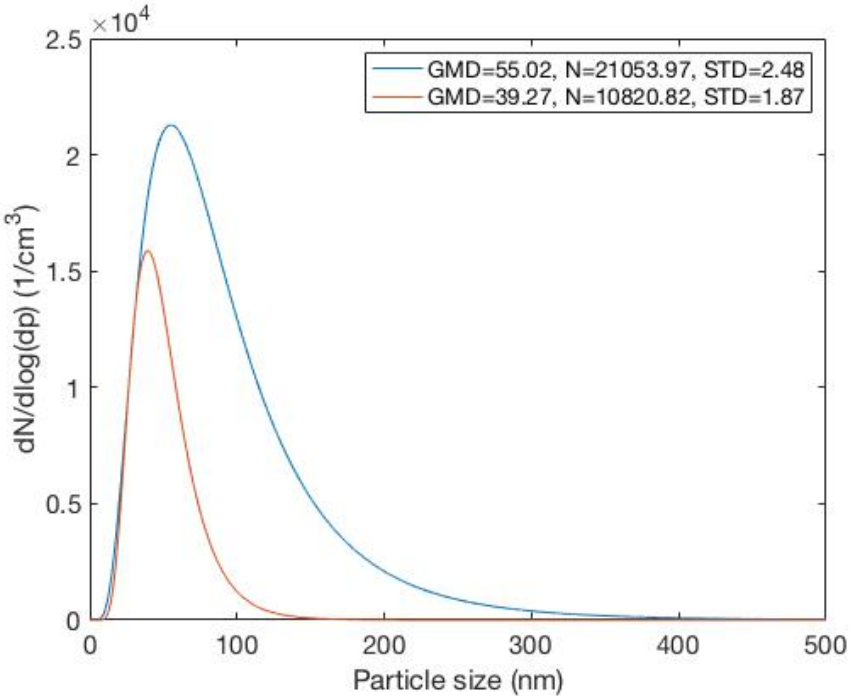

Figure 6. Upper (blue) and lower (red) limit size distributions for 25 and 26 October determined from size distributions between 18 and 20 October 2014. Values for the parameters used are shown in the legend.

Updraft velocities

Vertical doppler velocities were used for determining updraft velocities. The parameterization model uses updraft velocities, because they influence the rate of change of supersaturation inside the rising parcel, as described by Eq. 3.

The doppler measurements of velocity that is used is an aggregation of data from cloud radar, lidar and a numerical forecast model, retrieved from Cabauw. For determining the updraft velocity, the method described by Rosenfeld et al. (2016) was used, in which only positive

vertical velocities are considered from a dataset of vertical doppler velocities. From the 30 seconds resolution measurements of vertical doppler, 10-minute averages were taken. For obtaining the updrafts at cloud base, the average of the positive vertical velocities at the first 50 meters of the cloud base was taken. Fig. 7 shows the obtained updraft velocities during 25 and 26 October.

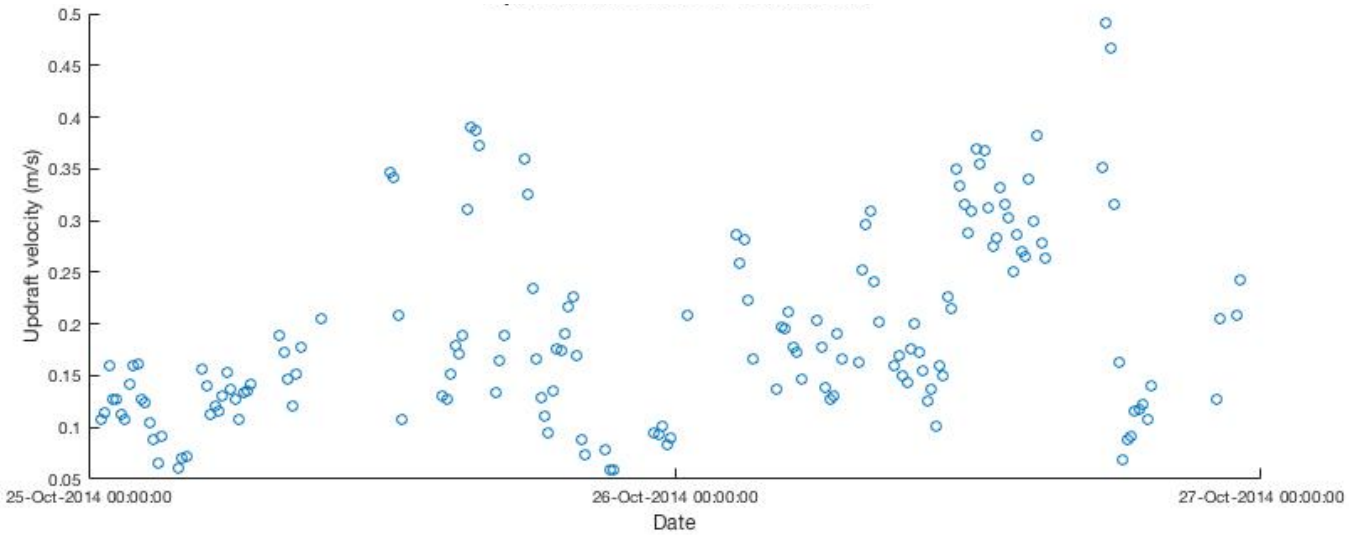

Figure 7. Updraft velocities determined from doppler velocities at cloud base height.

Hygroscopicity

Hygroscopicity values were obtained from a Hygroscopic Tandem Differential Mobility Analyser (HTDMA) that was placed at Cabauw during the ACCEPT campaign. This HTDMA measured hygroscopicities for particles having sizes of 60, 80, 100, 140 and 180 nm. Since the measured hygroscopicities showed weak dependency with particle size, the average hygroscopicity over all sizes was taken as input for the parameterization model. Fig. 8 shows the evolution the hygroscopicity.

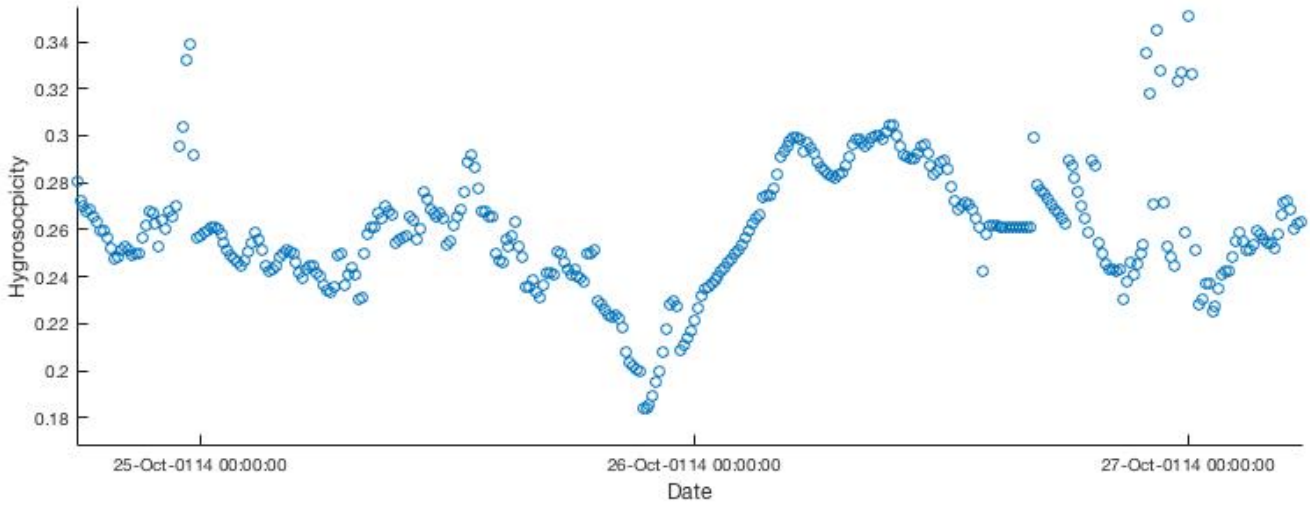

Figure 8. Hygroscopicity measurements during 25 and 26 October

3. RESULTS AND DUSCUSSION

3.1 Sensitivity analysis

As it is visible from the input data of updraft velocities in Fig. 7, updraft velocities change rapidly but are essentially confined to the range between 0.1 m/s to 0.35 m/s. This variability is excessively reflected in the Nenes CDNC (Fig. 9), where the droplet concentrations vary between 100 and 900 cm^{-3} (yellow curve). On the other hand, the CDNC only shows small changes in the range of 10 droplets/cm^{-3} when the updraft velocity is kept at constant values (red and blue curve). The constant values used for the updraft velocity w are given by:

$w_{high} = \mu_w + \sigma_w$

$w_{low} = \mu_w - \sigma_w$

expressed through the mean (μ_w) and the standard deviation (σ_w) of the observations.

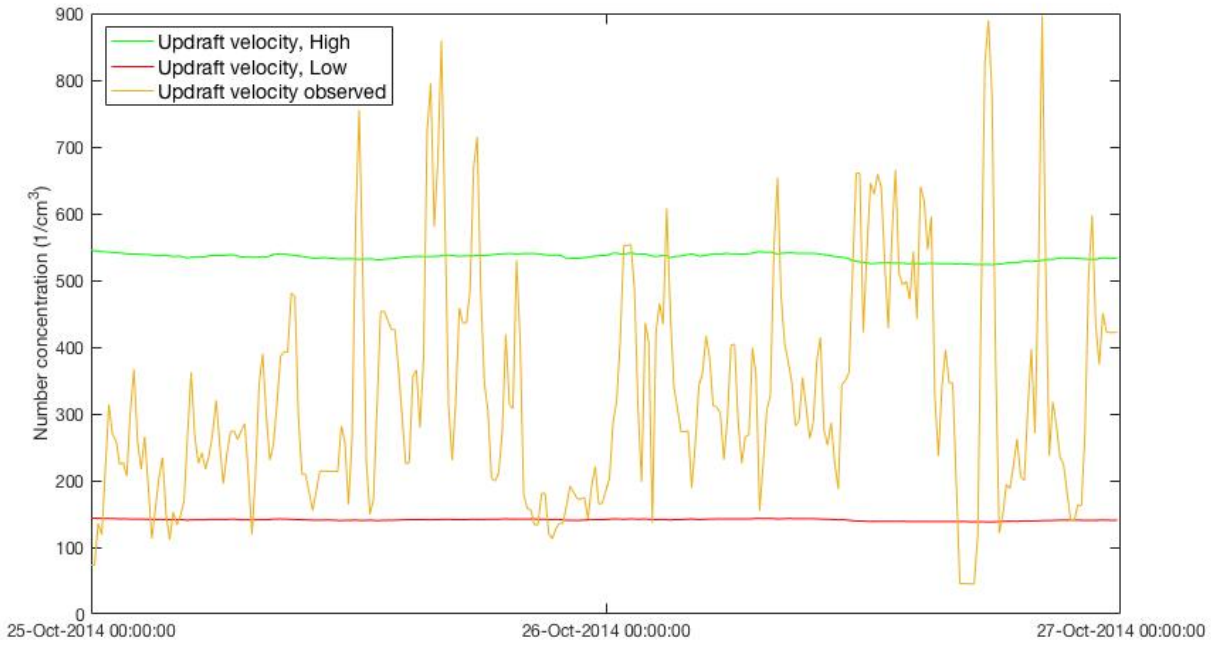

Figure 9. Sensitivity analysis of updraft velocity. Nenes CDNC obtained from setting high (green) and low (red) boundary vertical velocity of respectively $w_{high} = 0.29$ m/s and $w_{low} = 0.07$ m/s. The yellow plot shows the Nenes CDNC that is obtained from using observed variations of updraft velocity (as shown in Fig 7).

From Fig. 9, it can be seen that the magnitude of updraft velocity plays a decisive role for the number of produced cloud droplets that is determined by the model, and that temporal changes of the other input parameters don't affect CDNC significantly. For high updrafts, a high amount of CDNC is produced, because the magnitude of supersaturation is higher as vertical velocity increases. The higher the supersaturation, the broader is the activation domain for the particle size distribution, which explains higher cloud droplet concentrations.

It can be derived that the cloud droplet number concentration is also quite insensitive to temperature, pressure, relative humidity and hygroscopicity. By keeping the vertical velocity constant, changes in CDNC are only caused by the other changing variables. Only minuscule changes in droplet concentration are obtained in this way, in the range of 10 droplets/cm^3. Updraft velocity variations is therefore the main driver for the CDNC variations over time.

Figure 10 shows the change of cloud droplet number concentration with respect to hygroscopicity at different updraft velocities.

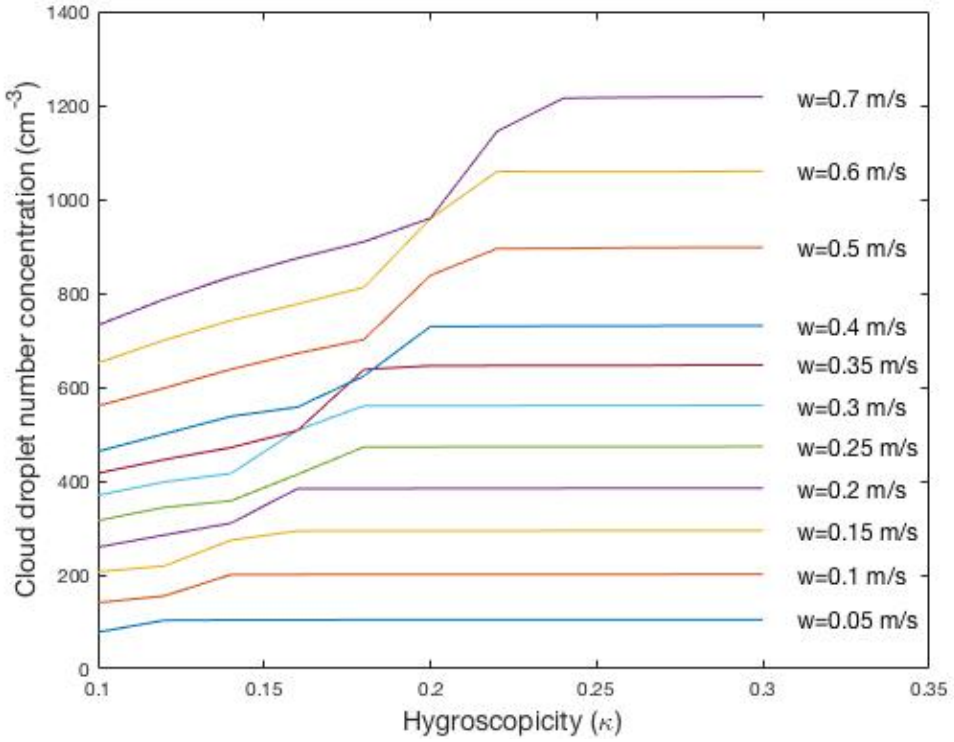

Figure 10. CDNC dependency on the hygroscopicity parameter at different updraft velocities, using the size upper boundary distribution (Fig. 5, blue curve).

It can be seen that the hygroscopicity becomes more important for particle activation as updraft velocity increases. This can be explained as follows:

The critical supersaturation (S_c) is obtained by setting dS_{eq}/dd_p of the Köhler relationship (Eq.1) to zero, which gives:

$$S_c = \left(\frac{4A^3}{27\kappa}\right)^{\frac{1}{2}} {d_p}^{-\frac{3}{2}} \qquad \text{Eq. 11}$$

The κ derivative of S_c in Eq. 11 expresses the change of the critical supersaturation with hygroscopicity:

$$\frac{\partial S_c}{\partial \kappa} = \frac{1}{2}\left(\frac{4A^3}{27}\right)^{\frac{1}{2}} {d_p}^{-\frac{3}{2}} \kappa^{-\frac{3}{2}} \qquad \text{Eq. 12}$$

This change is large, if the dry particle diameter (d_p) is small, and it is small if d_p is large. In other words, the activation of small particles is more strongly promoted by their hygroscopicity than the activation of large particles.

Since at large updraft velocities, the supersaturation becomes higher (Eq. 4 and 5), and small particles play a larger role at higher supersaturations (Köhler relationship, Eq. 1), it can be concluded that hygroscopicity is more important at high updraft velocities, explaining this effect seen in Fig. 10.

The graph demonstrates that at typical observed updraft velocities that range from 0 to 0.4 m/s (Fig. 7), hygroscopicities above 0.2 don't play a significant role in the formation of cloud droplets. Since the large majority of the hygroscopicity measurements (Fig. 8) are above this value, it can be concluded that hygroscopicity plays an insignificant role in the formation of cloud droplet for the observed data.

3.2 Cloud droplet number concentration Comparison

As can be seen in Fig. 11a and 11b, both the upper and the lower limit of the Nenes CDNC is in most cases below the remote sensing CDNC. For the upper limit (blue curve), the averaged relative errors between the models (considering each point in time separately) are 44.6 % and 41.1 % respectively for 25 and 26 October. For the lower limit (orange curve), the relative errors between the models are 67.8 % and 78.0 % respectively for 25 and 26 October.

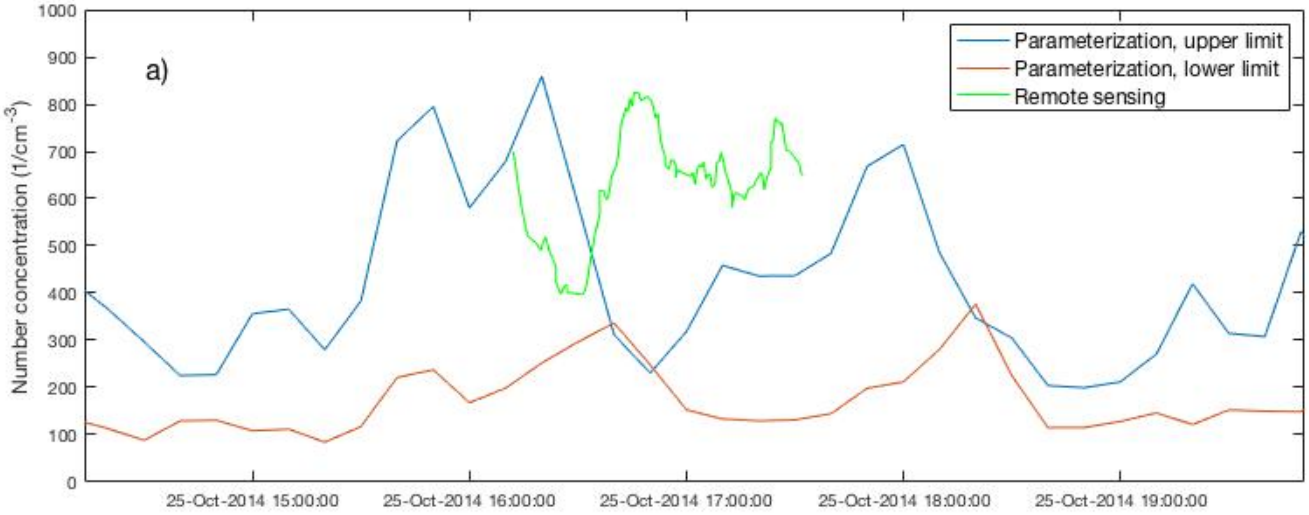

Figure 11a. CDNC determined by the parameterization model plotted against CDNC determined by remote sensing method for 25 October. CDNC that correspond with upper and lower size distribution limits are shown (see Eq. 10a and b and Fig. 6).

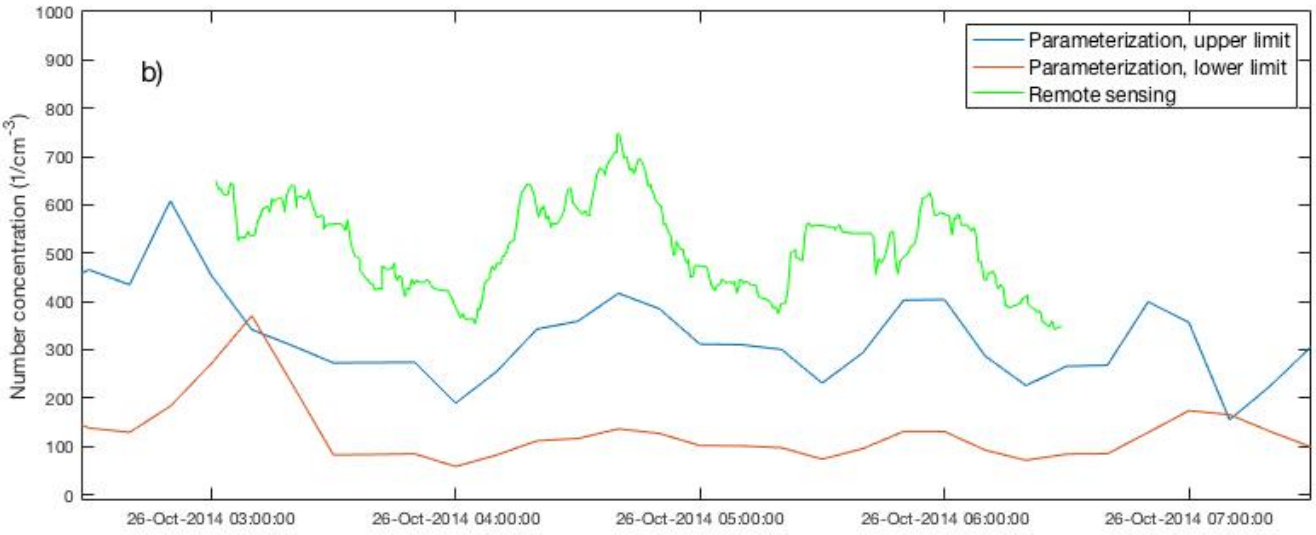

Figure 11b. CDNC determined by the parameterization model plotted against CDNC determined by remote sensing method for 26 October. CDNC that correspond with upper and lower size distribution limits are shown (see Eq. 10a and b and Fig. 6).

The concentration of cloud droplets directly influences the scattering properties of the cloud. It is therefore important to know how much an error CDNC influences an error in the scattering intensity. The relationship between scattering intensity (I/I_0) and droplet size (D_p) is described by the Mie Theory, see Appendix, where the scattering intensity is proportional to D_p^2. Assuming a number of n droplets in the cloud that each scatter light, this relationship can be simplified to:

$$\frac{I}{I_0} \sim D_p^2 \, n \qquad \text{Eq. 13}$$

The total volume (V) of liquid water in the cloud can be approximated as the sum of all individual volumes of n monodisperse cloud droplets:

$$V = n \, \frac{\pi}{6} D_p^3 \qquad \text{Eq. 14}$$

Assuming that the liquid water content in the cloud is constant, then V is constant. By substituting the D_p of Eq. 14 into Eq. 13, the following relationship is obtained (omitting the constant parameters):

$$\frac{I}{I_0} \sim N^{\frac{1}{3}} \qquad \text{Eq. 15}$$

For a relative error of CDNC that ranges between 0.41 and 0.78, as obtained from the Nenes model, a relative error of scattering intensity can be found in approximately the range of 0.13 and 0.26. The error in the predicted CDNC therefore leads to an error of scattering intensity that is smaller.

As can be seen in Fig. 11a and b, the errors in the determined CDNC appear to be systematic for some cases, in which the Nenes CDNC and remote sensing CDNC follow approximately similar trends. The results of the 25th suggest a time lag of about 1 hour between the upper limit of Nenes determined CDNC and the remote sensing CDNC curve, whereas for the results of the 26th a vertical shift of 300 particles/cm^3 is recognizable. Since the Nenes CDNCs show a different pattern to the remote sensing CDNCs for each day, the results from 25 and 26 October are discussed separately in the following.

25 October 2014

One could hypothesize that a possible cause for the horizontal shift in Fig 11a could be due to a delay of the parcel arriving at cloud base height. Particles inside an air parcel moving up from ground level to a cloud base height of 1000m with a vertical velocity of 0.2 m/s will take 1.4 hours to be converted to cloud droplets. Shifting the CDNC from Nenes model by 1.4 hours forward would indeed improve the correspondence in Fig. 11a.

However, this hypothesis proves to be faulty considering the input settings that are used for the simulations that were done for this comparison. For this comparison, particle size distributions are kept at constant values, which means that variations in CDNC over time due to changing size distributions can be excluded. Neither can the variations in CDNC be explained by variations in hygroscopicity, since, as shown in the sensitivity analysis, hygroscopicity has a negligible influence on the cloud droplet formation at vertical velocities in the measured range (0.0 – 0.4 m/s). Variations of temperature, pressure, relative humidity also don't play a significant role for the CDNC variations as seen in the sensitivity analysis. It is mainly the updraft velocity at cloud base height that is responsible for CDNC variations. Since vertical velocity measurements are obtained at cloud base height, their effect on the CDNC is immediate, and therefore the horizontal shift seen in Fig. 11a cannot be explained with a time lag. A possible reason for the discrepancies seen in Fig. 11a is therefore an error in the determination of the updraft velocity during 25 October.

For the same reason as that no time shift is expected, horizontal wind is expected to have only little influence on the predicted cloud number concentration. Ground measured input parameters that have only little effect on CDNC variations are used, which will not cause variations of CDNC for different horizontal wind velocities.

26 October

For 26 October (Fig. 11b), the input parameters (mainly the vertical velocity) appear to cause a CDNC upper limit that is approximately a factor of 2 apart from the remote sensing CDNC for each point in time.

The Nenes model assumes that ground-measured size distributions are the same as the size distributions at cloud base height. This is a rough approximation, since particles in a rising parcel will undergo chemical reactions with trace gasses (particle ageing) and water will be deposited even before they reach the cloud base height. This causes the size distribution to shift towards accumulation mode sizes, and the size distribution at cloud base height is in reality larger than it is set in the Nenes model. A larger particle size reduces the critical supersaturation that the particles need to be activated, as can be seen in the Köhler theory, and therefore enhance cloud droplet formation. This could be a reason that the CDNC is higher in reality than it is predicted by Nenes model. A particle that did not have the potential of becoming a CCN at ground level, might have changed into a potential CCN at cloud base height.

Furthermore, the hygroscopicity of the rising particles will most probably increase through these ageing reactions (Trischer et al., 2011) and through the deposition of water on the way towards the cloud. However, as seen in the sensitivity analysis, a further increase from the 0.2 ground-measured hygroscopicity would not significantly influence the production of cloud droplets for the obtained updraft velocities. This would mean that an increased CDNC as a result of particle ageing would only be caused by the growth of particles, and not by an increased hygroscopicity.

As Fig. 11b suggests, the parameterization model systematically underestimates the CNDC for 26 October. Therefore, a different size distribution was used in the following as input for the parameterization for this day. This size distribution was chosen as such to obtain a CDNC that agrees best with the remote sensing observations (see Fig. 12). The relative error between of the Nenes CDNC and the remote sensing CDNC, considering at each point in time separately, is herein averaged 15.5%.

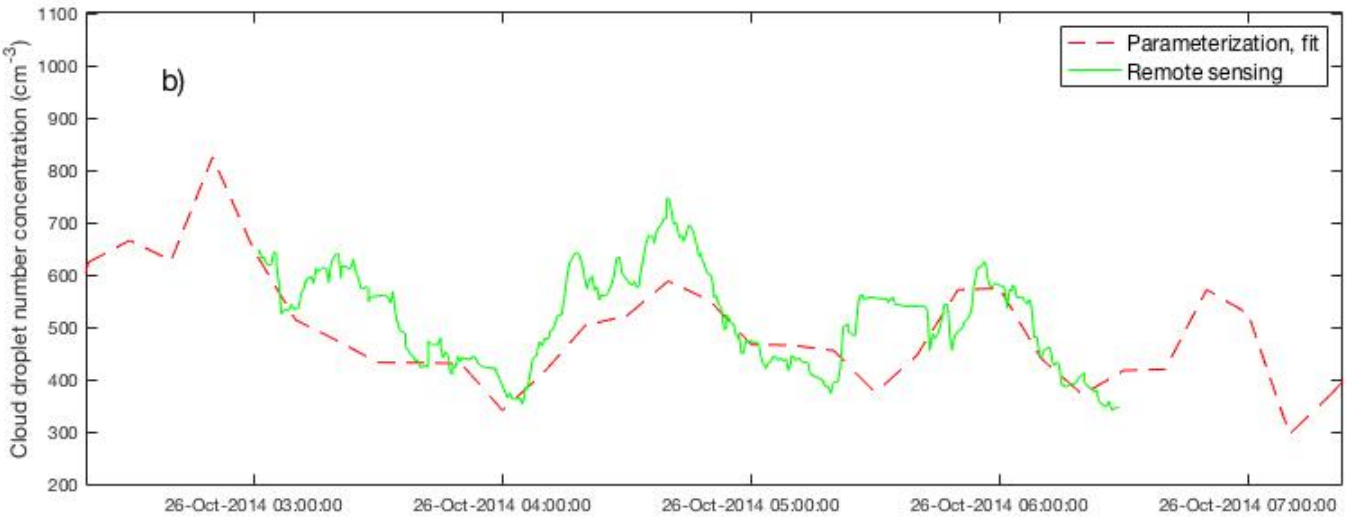

Figure 12. CDNC determined by the parameterization model plotted against CDNC determined by remote sensing method for 26 October. The input values of the particle size distribution are chosen as such, that the CDNC from the parameterization model has the best fit to the CDNC obtained by remote sensing method.

For obtaining this fit, the geometric mean diameter (GMD) and the total number concentration (N) parameters of the size distribution were changed such that the Nenes CDNC corresponds to the remote sensing CDNC, keeping the standard deviation constant at μ_{STD}. Changing these two parameters yields a variety of GMD and N combinations that yield the same Nenes CDNC, as shown in Figure 13. The blue dotted line represents the average value of remote sensing CDNC on 26 October. The intersection between the dotted line and the colored curves therefore reveals the GMD and N values that are needed for obtaining a similar CDNC to the remote sensing one using Nenes parameterization model.

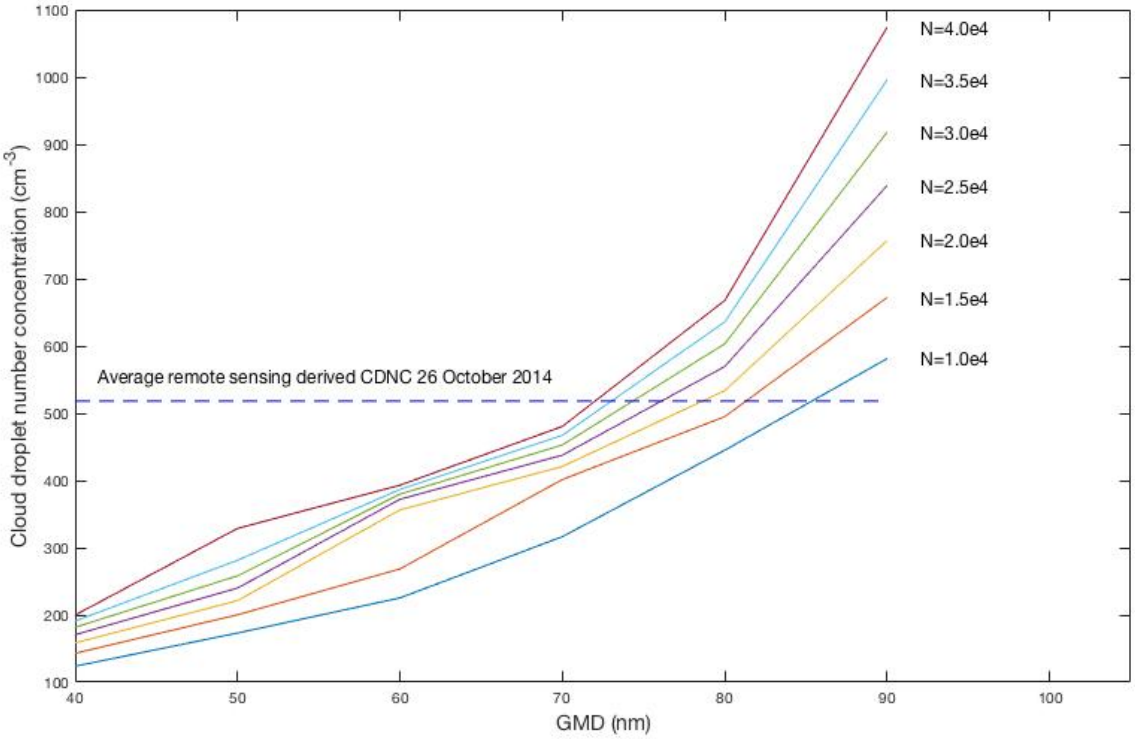

Figure 13. Dependency of Nenes CDNC on the geometric mean diameter (GMD) and total number concentration (N) parameter values of the particle size distribution, keeping the STD parameter constant at μ_{STD}. The dotted line is the average remote sensing CDNC on 26 October.

The intersections in the graph show that in order for the Nenes CDNC to correspond to the remote sensing CDNC, the geometric mean diameter of the size distribution has to be at least 70 nm. A GMD of this magnitude is 3 standard deviations higher than the mean of the observed GMDs on the days 18-20 October (see Fig. 5a). Values that are 3 standard deviations off the mean are highly improbable, and therefore it is unlikely that that such size distributions prevail few days later on 25 and 26 October.

Therefore, the input parameter "size distribution" for Nenes model is ruled out as (the only) responsible factor for the underestimation of CDNC.

4. CONCLUSION

The current research was done to compare the results of two fundamentally different methods for determining the cloud droplet number concentration. The one is based on optical measurements from remote sensing devices, and utilizes the theories of particle-light interactions for determining the CDNC. The other method is by far more indirect than the first one, in which the theory of droplet growth is applied to ground-measured particle size distributions. The comparison done shows that, despite the methods being fundamentally different from each other, in all measurements the obtained CDNC lies in the same order of magnitude and the temporal variability of CDNC corresponds at least for the comparison of 26 October.

Both the magnitude of updraft velocities and the distribution of the ground measured particles was found to have the largest influence on the magnitude of cloud droplet number concentrations. To investigate whether the discrepancies between the predicted and observed CDNC could be caused by a faulty size distribution assumption, it has been shown that the discrepancies can only be solved when using an unrealistic size distribution as input parameter. Since this size distribution is unlikely to occur, it can be concluded that the size distribution input cannot be the main cause for the discrepancies of the seen magnitude. The remaining parameter held to be responsible for the discrepancies is therefore the updraft velocity. Either the CDNC computation from updraft velocities is faulty, or the input updraft velocities are inaccurate.

Relative errors in the CDNC ranged between 0.41 and 0.78. These errors lead to relative errors for scattering intensity in the range of 0.13 and 0.26, respectively. Given the fact that an error in CDNC leads to an error in scattering intensity that is lower, implies that a highly accurate determination of CDNC might not even be necessary in order to obtain scattering intensities that are in proximity of the true values. Therefore, a simplified model such as the Nenes parameterization that shows some discrepancies in determined CDNC, might even be sufficient to capture the indirect effect that aerosols have on incoming radiation.

Furthermore, as has been shown in the sensitivity analysis, hygroscopicity plays a negligible role for cloud droplet formation during the two measurement days at Cabauw. But as has also shown, hygroscopicity plays a larger role for the formation of cloud droplets for smaller particle sizes. So, it is to be expected that if the particle size is much smaller than it is typically measured at the Cabauw station, hygroscopicity plays a much more important role. Hygroscopicity can change over height caused by atmospheric chemistry with anthropogenic pollutants. This leads to formation of hygroscopic species that condense on particles, which can increase hygroscopicity. Implementing hygroscopicity measurements taken from higher altitudes into the Nenes model would therefore increase its performance. Height-resolved measurements of hygroscopicity will be possible thanks to recent development in light-weight differential

mobility analyzers (DMA), which can measure hygroscopicity if they are set up as tandem DMAs (Bezantakos, Huang, Barmpounis, Martin & Biskos, Bezantakos, Huang, Barmpounis, Martin & Biskos, 2016).

Moreover, in a future study, it would be desirable to represent the Nenes CDNC with an added spatial component. Recent studies have shown that the low-priced and light-weight Alphasense N2-OPC measures size distributions in approximate accordance to measurements of the Grimm OPC at high altitude conditions (Bezantakos, Schmidt-Ott & Biskos, 2018; Gu, Michanowicz & Jia, 2018). Therefore, by using unmanned aerial vehicles (UAVs) for size distribution measurements, tempo-spatially resolved Nenes CDNC can be obtained in an economic way.

5. APPENDIX

The integral diameter in s_c space is defined as:

$$I(0,s) = \int_0^s n(s_c) D_P(s_c, t) ds_c \qquad \text{Eq. 16}$$

where $n(s_c)$ is the aerosol size distribution that is mapped to the critical supersaturation space and D_p is the droplet diameter (Morales Betancourt et al., 2014).

Furthermore,

$$\alpha = \frac{g M_w \Delta H_v}{c_p R T^2} - \frac{g M_a}{RT} \qquad \text{Eq. 17}$$

$$\gamma = \frac{p M_a}{p^s M_w} - \frac{M_w \Delta H_v^2}{c_p R T^2} \qquad \text{Eq. 18}$$

where p is atmospheric pressure, g is acceleration due to gravity, R is the gas constant, c_p is the specific heat of air and M_a and M_w is the molecular weight of dry air and water, ΔH_V is the latent heat of condensation of water and T is the parcel temperature (Nenes & Seinfeld, 2003).

The scattering intensity is given as:

$$I(\theta) = \frac{I_0 {D_p}^2 i}{4\pi^2 R^2} \qquad \text{Eq. 19}$$

where I_0 is the intensity of incoming light, D_p is the particle diameter, R is the distance and i is the Mie scattering intensity parameter for light with perpendicular or parallel polarization, which is a function of the scattering angle θ. (Hinds, 1999)

Figure 14 shows two examples of less perfect dN/dlog(dp) fits. In both fits the problem occurs that the size distributions consist of multible overlapping fit size distributions, which the fit doesn't account for.
As seen in the second graph, large particle sizes (which can play an important role as water vapor sink, consuming far more than other particles) are highly underestimated.

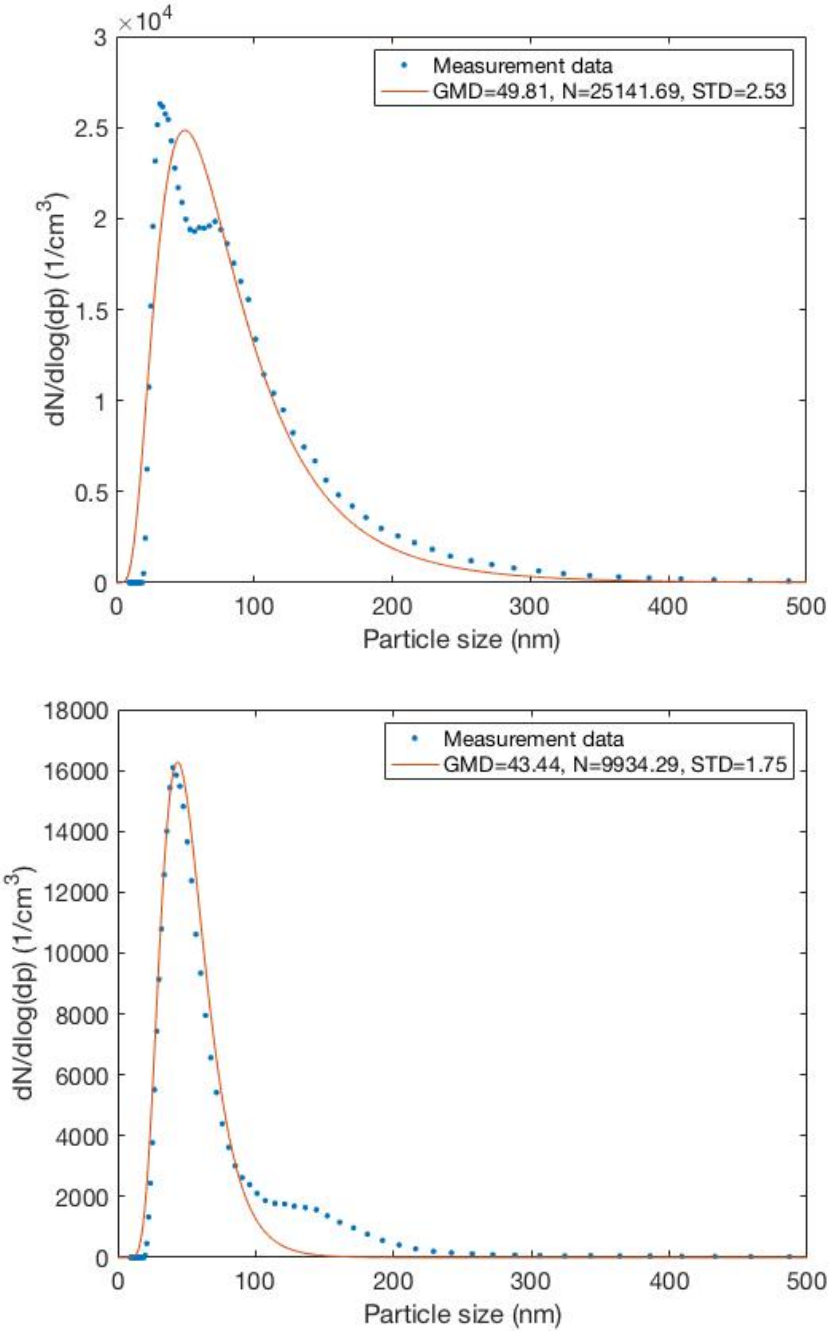

Figure 14. Examples of two less perfect fits than the one shown in Fig. 4. The size distributions are measured on 18 October 2014, 18:00 (first graph) and on 20 October 2014, 00:00 (second graph).

REFERENCES

Bezantakos, S., Huang, L., Barmpounis, K., Martin, S. T., & Biskos, G. (2016). Relative humidity non-uniformities in Hygroscopic Tandem Differential Mobility Analyzer measurements. Journal of Aerosol Science, 101, 1-9.

Bezantakos, S., Schmidt-Ott, F., & Biskos, G. (2018). Performance evaluation of the cost-effective and lightweight Alphasense optical particle counter for use onboard unmanned aerial vehicles. *Aerosol Science and Technology*, *52*(4), 385-392.

Cimatti, G. (1991). Existence and uniqueness for the equations of the Joule-Thomson effect. *Applicable Analysis*, *41*(1-4), 131-144.

Fountoukis, C., Nenes, A., Meskhidze, N., Bahreini, R., Conant, W. C., Jonsson, H., ... & Flagan, R. C. (2007). Aerosol–cloud drop concentration closure for clouds sampled during the International Consortium for Atmospheric Research on Transport and Transformation 2004 campaign. *Journal of Geophysical Research: Atmospheres*, *112*(D10).

Friedlander, S. K. (1977). Smoke, dust and haze: Fundamentals of aerosol behavior. *New York, Wiley-Interscience, 1977. 333 p.*

Ghan, S. J., Abdul-Razzak, H., Nenes, A., Ming, Y., Liu, X., Ovchinnikov, M., ... & Shi, X. (2011). Droplet nucleation: Physically-based parameterizations and comparative evaluation. *Journal of Advances in Modeling Earth Systems*, *3*(4).

Griffin, R. J. (2013). The sources and impacts of tropospheric particulate matter. *Nature Education Knowledge*, *4*(5), 1.

Gu, Q., R Michanowicz, D., & Jia, C. (2018). Developing a Modular Unmanned Aerial Vehicle (UAV) Platform for Air Pollution Profiling. *Sensors*, *18*(12), 4363.

Hinds, W. C. (1999). Aerosol technology: Properties, behavior, and measurement of airborne particles. New York: Wiley.

IPCC, 2014: *Climate Change 2014: Synthesis Report*. *Contribution of Working Groups I, II and III to the Fifth Assessment Report of the Intergovernmental Panel on Climate Change* [Core Writing Team, R.K. Pachauri and L.A. Meyer (eds.)]. IPCC, Geneva, Switzerland, 151 pp.

Joule, J. P., & Thomson, W. (1852). LXXVI. On the thermal effects experienced by air in rushing through small apertures. *The London, Edinburgh, and Dublin Philosophical Magazine and Journal of Science*, *4*(28), 481-492.

Meskhidze, N., Nenes, A., Conant, W. C., & Seinfeld, J. H. (2005). Evaluation of a new cloud droplet activation parameterization with in situ data from CRYSTAL-FACE and CSTRIPE. *Journal of Geophysical Research: Atmospheres*, *110*(D16).

Morales Betancourt, R., & Nenes, A. (2014). Droplet activation parameterization: The population-splitting concept revisited. *Geoscientific Model Development*, *7*(5), 2345-2357.

Nenes, A., & Seinfeld, J. H. (2003). Parameterization of cloud droplet formation in global climate models. *Journal of Geophysical Research: Atmospheres*, *108*(D14).

Nenes, A., Ghan, S., Abdul-Razzak, H., Chuang, P. Y., & Seinfeld, J. H. (2001). Kinetic limitations on cloud droplet formation and impact on cloud albedo. *Tellus B: Chemical and Physical Meteorology*, *53*(2), 133-149.

Peng, Y., Lohmann, U., & Leaitch, R. (2005). Importance of vertical velocity variations in the cloud droplet nucleation process of marine stratus clouds. *Journal of Geophysical Research: Atmospheres*, 110(D21).

Rosenfeld, D., Zheng, Y., Hashimshoni, E., Pöhlker, M. L., Jefferson, A., Pöhlker, C., ... & Fischman, B. (2016). Satellite retrieval of cloud condensation nuclei concentrations by using clouds as CCN chambers. *Proceedings of the National Academy of Sciences*, *113*(21), 5828-5834.

Rusli, S. P., Donovan, D. P., & Russchenberg, H. W. (2017). Simultaneous and synergistic profiling of cloud and drizzle properties using ground-based observations. *Atmospheric Measurement Techniques*, *10*(12).

Snider, J. R., Guibert, S., Brenguier, J. L., & Putaud, J. P. (2003). Aerosol activation in marine stratocumulus clouds: 2. Köhler and parcel theory closure studies. *Journal of Geophysical Research: Atmospheres*, *108*(D15).

Thomson, W. (1872). 4. On the equilibrium of vapour at a curved surface of liquid. *Proceedings of the Royal Society of Edinburgh*, *7*, 63-68.

Tritscher, T., Jurányi, Z., Martin, M., Chirico, R., Gysel, M., Heringa, M. F., ... & Baltensperger, U. (2011). Changes of hygroscopicity and morphology during ageing of diesel soot. *Environmental Research Letters*, *6*(3), 034026.

Twomey, S. (1977). The influence of pollution on the shortwave albedo of clouds. *Journal of the atmospheric sciences*, *34*(7), 1149-1152.

Wallace & Hobbs (2006), Atmospheric Science: An Introductory Survey. Amseterdam: Elsevier Academic press.

Yau, M.K. and Rogers, R.R. (1989) Short Course in Cloud Physics. 3rd Edition, p.84

Zieger, P., Fierz-Schmidhauser, R., Weingartner, E., & Baltensperger, U. (2013). Effects of relative humidity on aerosol light scattering: results from different European sites. *Atmospheric Chemistry and Physics*, *13*(21), 10609-10631.